Collagen Matrix in Development and Progression of Experimentally Induced Respiratory Neoplasms in the Hamster

Jaakko Laitakari and Frej Stenbäck

Toxicol Pathol 2001 29: 514
DOI: 10.1080/019262301317226311

TOXICOLOGIC PATHOLOGY, vol 29, no 5, pp 514–527, 2001

Collagen Matrix in Development and Progression of Experimentally Induced Respiratory Neoplasms in the Hamster

JAAKKO LAITAKARI AND FREJ STENBÄCK

Department of Pathology, University of Oulu, Kajaanintie 52D, 90220 Oulu, Finland

ABSTRACT

Intratracheal instillations of 7H-dibenzo(c, g)carbazole (DBC), a tobacco smoke component, into Syrian golden hamsters, resulted in preneoplastic lesions and benign and malignant respiratory neoplasms. Neoplastic progression was associated with specific changes in the extracellular matrix (ECM), dependent on the stage of tumor development. DBC-induced tracheobronchial squamous metaplasia was associated with an increase in collagen type I and type III deposition in the subepithelial ECM, as observed by computer-assisted image analysis of immunohistochemical staining for the aminoterminal propeptides of collagen type I (PINP) and collagen type III (PIIINP). Increased collagen matrix synthesis was detected in dysplasia by in situ hybridization of α1(I) mRNA for collagen I and α1(III) mRNA for collagen type III after continued exposure to DBC. In well-differentiated squamous cell carcinomas with an expansive growth pattern, collagen deposition increased, as did fiber size. In moderately differentiated neoplasms, basement membrane (BM) destruction and invasion was associated with a destructive growth pattern and decreases in collagen synthesis and the deposition of new collagen. Preserved deposition of mature collagen was detected by staining for the telopeptide of collagen type I propeptide. In less differentiated tumors, ECM development was minimal, with few and small fibers, possibly explaining the rapid development of these neoplasms. Transforming growth factor β (TGFβ1) immunoreactivity was increased in hyperplastic epithelium and well differentiated neoplasms and decreased in dysplasia and less differentiated squamous cell carcinomas, while TGFβ2 and TGFβ3 expression was also distinct in neoplastic cells. Collagen synthesis and epithelial differentiation were associated with an increased number of myofibroblasts in the ECM and with increased TGFβ3 immunoreactivity in differentiated cells and in the matrix. The nature of the composition of the ECM was related to neoplastic growth and progression when analyzed by computer-associated image analysis, revealing alterations in collagen structure, size, and shape.

Keywords. Morphometry; automated image analysis; extracellular matrix; collagens; lung carcinogenesis; lung tumors.

INTRODUCTION

Studies of the causes, pathogenesis, development and behavior of human respiratory neoplasms pose problems inherent to the nature of these tumors. They are rapidly fatal if untreated and ethical considerations prevent any follow-up of uninterrupted neoplastic progression. The hamster intratracheal instillation model (51) has been shown to be effective in producing tumors similar to those found in man (60). When given with ferric oxide (Fe_2O_3), polycyclic hydrocarbons, including benzo (a) pyrene (B(a)P), cause a high incidence of respiratory tract tumors (23, 36, 51, 52, 56, 57, 60). Because 7H-dibenzo[c,g]carbazole (DBC) also induces a high incidence of malignant tumors in the upper and lower respiratory tract when given alone (57), we used this model to study the mechanisms of respiratory carcinogenesis, tumor induction, development and progression.

The role of exogenous agents in respiratory tumor induction has been extensively analyzed in epidemiological studies. However, less is known of the action of specific agents in the development and progression of these tumors. Hoffmann and Wynder (24) reported that smoke from 100 cigarettes contained 0.7 μg DBC and 3.9 μg BaP. The presence of DBC in tobacco tar and in petroleum combustion products (68, 69) makes this compound of interest in studies of human exposure to environmental agents.

Tracheobronchial and alveolar epithelial structures have received most attention in the study of respiratory carcinogenesis. The extracellular matrix (ECM) has been less considered, and then mainly as a supportive structure, although it actively participates in tumor development in many organs (26). The bulk of the collagen matrix consists of interstitial collagen types I and III (14, 44–47). The fiber-forming interstitial type I and type III collagens are synthesized as procollagens, containing propeptide domains at both ends of the molecule, that are usually cleaved off en bloc during secretion into the ECM (14, 46). The antibodies used in this study were against the aminoterminal propeptide of type I procollagen (PINP), and the aminoterminal propeptide of type III procollagen (PIIINP), also known as type I and type III pN collagen (33). PINP is mainly present in newly synthesized collagen containing the aminoterminal propeptide (72). Antibodies to the cross-linked carboxyterminal telopeptide of type I collagen (ICTP) can be used to measure cross-linked mature type I collagen in human tissue (44) and degradation products of collagen type I (34, 44). The antibody to collagen type III propeptide (PIIINP) binds to newly synthesized collagen, whose location and quantity are comparable to those of mature collagen (47, 73). In tissues, some of the type III collagen retains its aminoterminal propeptide when incorporated into fibers (13). Immunoassays for different collagen components as well as immunohistochemical studies on collagen expression have shown clinical usefulness in studies on neoplasms in different organs (26, 47, 64, 72, 73).

The occurrence and location of growth factors regulate many cellular functions, including cell proliferation and collagen deposition. Growth factors of the TGFβ family are highly potent growth regulators of epithelial cell proliferation and differentiation (4, 7, 8, 20, 49, 50, 59). In vivo,

Address correspondence to: Frej Stenbäck, Department of Pathology, University of Oulu, Aapistie 5, POB 5000, FIN 90014, Oulu, Finland; e-mail: frej.stenback@oulu.fi.

0192-6233/01$3.00+$0.00

TGFβ genes are expressed in embryonic epithelia undergoing critical stages of tissue morphogenesis and/or epithelial differentiation (12, 16, 22, 38). TGFβ also plays a crucial role in the regulation of cell proliferation, differentiation and chemotaxis (37, 39). Overexpression of TGFβ has been associated with malignant progression (20, 25) and an unfavorable prognosis of neoplasms (21). TGFβ regulates epithelial-mesenchymal interactions and acts as an endogenous regulator of epithelial homeostasis (20). It also accelerates wound healing (29). In vitro, TGFβ stimulates ECM production in response to external stimuli, including mitogens and differentiating agents (31). Through these profound effects on connective tissue biosynthesis, TGFβ may play a significant role in the development of normal and tumor stroma.

Analysis of specific cellular changes is feasible in immunohistochemical studies, allowing distinction of morphological entities. However, histoscores and similar systems are difficult to apply to large series with sufficient reproducibility, hindering statistical analysis of the results (5, 53). Computer-assisted image cytometry has been proposed as a means to solve these problems (17, 35) and it has gained acceptance in analysis of hormone receptors, cell proliferation (10, 40, 43), and ploidy (2). Clinical applications in tumor prognostication have also been proposed. Variability in automated image analysis occurs, and Reeder et al (42) reported significant differences to be due to specimen variability in sampling. Studies involving controlled conditions and defined endpoints are few.

In this study, we report on the role of matrix constituents and the significance of changes in collagen structure and location in relation to sensitivity as regards tumor formation, the structure of respiratory epithelium, as well as neoplasm development and behavior. The distribution and expression of newly formed collagen type I (via analysis of PINP), mature, cross-linked collagen type I (via ICTP), and newly formed collagen type III (via PIIINP) was studied by immunohistochemistry and compared with results obtained from staining of reticulin using conventional staining methods. Collagen synthesis was evaluated by in situ hybridization of collagen α1(I) mRNA, α2(I) mRNA, and α1(III) mRNA. The results were analyzed using computer-assisted image analysis in a CAS-200 system, providing a method for the detailed analysis of minor alterations in large numbers of cellular structures.

Materials and Methods

In this study, 192 8-week-old Syrian hamsters were divided into 4 groups as previously published (57). The animals were randomly bred in the Eppley colony, supervised by an animal control committee. The experiments were carried out according to standard procedures, following appropriate regulations. The chemical, DBC (Aldrich Chemical Co, Milwaukee, Wisconsin, USA), was 99% pure. Treatments were carried out as previously described (57). Group 1 received a weekly instillation of 3.0 mg DBC in 0.2 ml water for 10 weeks and group 2, 0.5 mg for 18 weeks. Group 3 received distilled water and group 4 was kept as an untreated control group. The animals were weighed weekly and allowed to die spontaneously or were sacrificed when moribund. At autopsy, the tracheas were ligated; the lungs, while still fully expanded, were removed en bloc and then fixed in 10% neutral-buffered formalin for an extended period of time.

Specimens

Paraffin-embedded specimens were cut five-μm-thick, and sections stained with hematoxylineosin and other stains, including periodic acid-Schiff (PAS), PAS after diastase treatment (dPAS), Mayer's mucicarmine, toluidine blue, and 1% alcian blue at different pHs. Masson's trichrome stain and van Gieson's stain were used to study the connective tissue components, acid-orcein-Giemsa stain to demonstrate elastic fibers, and Gomori's silver impregnation for reticular fibers.

Antibodies

The antibodies used are listed in Table 1 and the conditions of use in Table 2. Antibodies used in this study included polyclonal antibodies against human collagens, raised in rabbits (33, 44). Antibodies to PINP (0.428 mg IgG/ml) were prepared from the ascitic fluid of a patient with pancreatic carcinoma (33, 72). Antibodies to ICTP (0.104 mg IgG/ml) were prepared by using human bone as starting material (48). Antibodies to PIIINP (0.808 mg IgG/ml) were produced as described previously (33, 73). Cross-reactivity between human and hamster tissues was confirmed, using human and mouse tissues as controls. Antibodies to TGFβ were obtained commercially (Santa Cruz Biotechnology Inc, Santa Cruz,

TABLE 1.—Markers, antibodies and sources of origin.

Antibody	Marker	Supplier
Sc 146 TGFβ1	transforming growth factor β1	Santa Cruz Biotechnology, Santa Cruz, California, USA
Sc 90 TGFβ2	transforming growth factor β2	Santa Cruz Biotechnology, Santa Cruz, California, USA
Sc 82 TGFβ3	transforming growth factor β3	Santa Cruz Biotechnology, Santa Cruz, California, USA
PINP	aminoterminal propeptide of type I procollagen	J & L Risteli, Univ. of Oulu, Oulu, Finland
ICTP	crosslinked telopeptide of type I procollagen	J & L Risteli, Univ. of Oulu, Oulu, Finland
PIIINP	aminoterminal propeptide of type I procollagen	J & L Risteli, Univ. of Oulu, Oulu, Finland
Laminin	laminin	J & L Risteli, Univ. of Oulu, Oulu, Finland
CM5	p53	Novocastra, Newcastle, Great Britain
P10	PCNA	Dako Co, Glostrup, Denmark
SMA	smooth muscle antigen	Dako Co, Glostrup, Denmark
Ma 903	keratins 1, 5, 10, 14	Enzo Diagnostics, Farringdale, New York, USA
MNF 116	keratins 5, 6, 8, 17, 19	Dako Co, Glostrup, Denmark
Mac 6	keratins 6, 14, 15, 16, 18, 19	Triton Diagnostics, Alameda, California, USA

Further information in the Materials and Methods section.

TABLE 2.—Antibodies and their applications: characteristics, clonality, material, pretreatment and concentration.

Antibody	Clonality	Material	Pretreatment	Concentration
TGFβ1	Polyclonal	Paraffin	MW	1:50
TGFβ2	Polyclonal	Paraffin	MW	1:50
TGFβ3	Polyclonal	Paraffin	MW	1:50
PINP	Polyclonal	Paraffin	MW	1:50
ICTP	Polyclonal	Paraffin	MW	1:50
PIIINP	Polyclonal	Paraffin	MW	1:50
Laminin	Polyclonal	Paraffin	MW	1:50
CM5	Polyclonal	Paraffin	MW	1:1,000
PC10	Monoclonal	Paraffin	MW	1:20
SMA	Polyclonal	Paraffin	MW	1:50
Ma 903	Monoclonal	Paraffin	pepsin	1:50
MNF 116	Monoclonal	Paraffin	pepsin	1:100
Mac 6	Monoclonal	Paraffin	pepsin	1:1

Further information in the Materials and Methods section.

California, USA), and used according to the supplier's instructions. The antibodies were polyclonal IgG rabbit antibodies, non cross-reactive with other isoforms. The TGFβ1 antibody (sc 146) identified an epitope mapping at the carboxyterminal of TGFβ1 of human origin, identical to corresponding rodent sequence. As blocking peptide, TGFβ1 was obtained from Life Technologies (Gaithersburg, Maryland, USA). The TGFβ2 antibody, sc 90, also identified an epitope mapping at the carboxyterminus of TGFβ2 of human origin. The TGFβ3 antibody, sc 82, also identified an epitope mapping at the carboxyterminus of TGFβ3 of human origin, identical to corresponding mouse and chicken sequences. For comparison, the same TGFβ isomers were used as previously described (19). For β identification of myofibroblasts, antibodies to smooth muscle actin (SMA) (Dako Co, Glostrup, Denmark) were used according to the supplier's recommendations. Antibodies to p53 (CM5) were obtained from Novocastra (Newcastle, Great Britain) and proliferating nuclear antigen (PCNA) antibody PC10 was from Dako Co (Glostrup, Denmark). They were used as previously described (61). For identification of various cell types, commercially available antibodies against cytokeratins, Ma 903 (Enzo Diagnostics, Farringdale, New York, USA), MNF 116 (Dako Co, Glostrup, Denmark) and Mac 6 (Triton Diagnostics, Alameda, California, USA) were used according to the suppliers' instructions.

Immunohistochemical Methods

Immunohistochemistry and in situ hybridization were performed as described previously (19, 26, 27, 62). Several different immunohistochemical methods were used in the study, employing different experimental conditions as well as numerous controls at different steps. The applicability of the antibodies for hamster tissues was verified using different human, mouse and hamster tissues as controls.

In situ Hybridization

The probes used for in situ hybridization in this study were prepared for use in studies on humans (26, 27). These probes required fairly stringent conditions for adequate function. Hence human control tissues were also extensively used, giving comparable results. A 372-bp Pstl-Pvull fragment of the cDNA corresponding to part of the carboxyterminal propeptide domain of the human proα1(I) chain cloned in plasmid pHCAL1U, and a 379-bp Pstl-PStl fragment of the cDNA covering part of the triple-helical domain as well as the carboxyterminal telopeptide and propeptide parts of the human proα1(III) chain, cloned in plasmid pHFS3, were subcloned into the polylinker site of pGEM1 vectors (Promega, Madison, Wisconsin, USA). A 571-bp Xbal-Pstl fragment coding for part of the triple helical domain as well as for the carboxyterminal telopeptide and propeptide domains of the human proα2(I) chain cloned into plasmid Hf1131, was prepared by restriction enzyme digestion of the cDNA, and subcloned into the polylinker site of pBluescript (SK-) vectors (Stratagene, La Jolla, California, USA). The authenticity of the inserts was verified by sequencing (Pharmacia sequencing kit, Pharmacia, Uppsala, Sweden). A riboprobe transcription kit (Promega, Madison, Wisconsin, USA) was used for transcription. Sense and antisense RNA probes were labelled with ^{35}S UTP (Amersham, Little Chalfont, UK). The sense probes were used for detecting nonspecific binding of RNA to the tissue. All the solutions and glassware used with the RNA probes were pretreated with 0.1% diethylpyrocarbonate (Sigma Chemical Co, St. Louis, Missouri, USA).

In situ hybridization was carried out as described previously (27), using both radioactive and digoxigenin procedures. Formalin-fixed, paraffin-embedded tissue sections were deparaffinized and pretreated with 0.2 M HCl for 7 minutes at room temperature, followed by a 5-minute wash in water and digestion with proteinase K (1 mg/ml) (Boehringer Mannheim, Mannheim, Germany) in PBS, pH 7.2, for 30 minutes at 37°C.

The sections were then dipped in 0.2% glycine in PBS at room temperature and washed twice with PBS for 30 seconds and 5 minutes, respectively. The sections were acetylated in 0.5% acetic anhydride in 0.1 M triethanolamine for 10 minutes, at room temperature. After a 5-minute wash in PBS and dehydration in an increasing series of ethanol concentrations, the sections were allowed to air-dry for 2 hours, or overnight, at room temperature. Prehybridization was carried out with 50% formamide, 10% dextran sulfate, 0.3 M NaCl, 10 mM Tris-HCl, pH 8.0, 10 mM Na_3PO_4, 5 mM EDTA, 10 mM dithiothreitol, yeast tRNA (1 mg/ml), 0.02% (w/v) Ficoll, 0.02% (w/v) polyvinylpyrrolidone, and bovine serum albumin (0.2 mg/ml). Prehybridization took place at 50°C, for 2 to 3 hours. The sections were then washed in PBS, dehydrated, and air-dried. The hybridization mixture contained all the constituents of the prehybridization mixture plus the specific probe. The probe was denatured by boiling for 1 minute and then placed on ice, and 1 Hμ (40 U) of ribonuclease inhibitor (Promega, Madison, Wisconsin, USA) was added. A 40 μl aliquot of the hybridization mixture (containing approximately 3×10^6 cpm ^{35}S) was placed on each section, and the sections were covered with Parafilm (American National Can, Greenwich, CT, USA). Hybridization took place overnight at 50°C in a moist chamber. The sections were then washed 3 times, for 45 minutes each, at 50°C, in a buffer containing all of the constituents of the hybridization mixture except for dextran sulfate and tRNA. The slides were then washed in 0.5 M NaCl in 10 mM Tris-HCl, pH 7.5, and 1 mM EDTA at 37°C, for 15 minutes. The next wash contained 40 μg RNAse A/ml (Sigma Chemical Co, St. Louis, Missouri, USA) in the same buffer, to remove any nonspecifically bound single-stranded probe and the incubation was

continued for 30 minutes. Sections were then washed in 0.5 M NaCl in Tris-EDTA at 37°C for 15 minutes, rinsed in 0.3 M NaCl in 0.03 M sodium citrate for 15 minutes at 45°C and, finally, in 0.075 M NaCl, 0.0075 M sodium citrate for 15 minutes at 60°C. After the washes, the sections were dehydrated in a graded series of ethanol containing 300 mM ammonium acetate and were air-dried at room temperature, overnight. Hybridization was detected by autoradiography after dipping the slides into NTB-3 nuclear track emulsion (Eastman Kodak, Rochester, New York, USA), melted at 42°C and diluted 1:1 with 1% glycerol. After drying for 1 hour at room temperature, the slides were kept in desiccant-containing boxes at 4°C, for 8 to 14 days. The exposed slides were developed in distilled water, fixed in Kodak AGEFIX for 5 minutes, and rinsed in distilled water. The slides were counterstained with hematoxylin and eosin.

The digoxin modification was otherwise similar except that digoxigenin-11-uridine-5-triphosphate was used as substrate and for RNA labeling to replace UTP in in vitro localization, and Fast-Red tablets were used for signal detection. The NTP labeling mixture contained 10 mM ATP, GTP, CTP each, and 6.5 mM UTP, 3.5 mM digoxigenin-3-O-methylcarbonyl-ε-aminocaproyl-[5-(3-aminoallyl)uridine-5′-phosphate]tetralithium salt in Tris-neutralized solution, ph7,5 (Boehringer-Mannheim, Mannheim, Germany). For detection of digoxin-labeled compounds anti-digoxin-AP, fragments were used. For this purpose Fab fragments from an anti-digoxigenin antibody from sheep was conjugated with alkaline phosphatase (AP) (Boehringer-Mannheim, Mannheim, Germany). After immunization with digoxigenin the sheep IgG was purified by ion exchange chromatography and the specific IgG was isolated by immunoabsorption. The Fab fragments obtained by papain digestion were conjugated with AP and stabilized in 50 mM triethanolamine buffer, 3mM NaCl, 1 mM MgCl2, 1% bovine serum albumin, pH 7.6. Subsequently dilution in 100 mM NaCl, pH 7.5 was performed. For detection Fast Red tablets containing 0.5. mg. naphtol substrate, 2 mg. Fast Red Chromate and 0.4 mg of levamisole as inhibitor of endogenous alkaline phosphatase were used.

Transmission Electron Microscopy

Fresh tissue was fixed in 3% glutaraldehyde in 0.1 M phosphate buffer, pH 7.4, postfixed in 1% osmium tetroxide in the same buffer, dehydrated in acetone and embedded in Epon LX 112. Sections of 1 μm were cut and stained with 1% toluidine blue for orientation by light microscopy. Ultrathin sections were cut with a Reichert Ultracut E-ultramicrotome (Reichert-Jung, Vienna, Austria), stained with uranyl acetate and lead citrate, and examined in a Philips TEM 410 LS transmission electron microscope.

Morphometry

Quantitative densitometry was performed using a CAS200 (Becton-Dickinson, Leiden, The Netherlands) automated image analyzer and the proprietary software, which was modified for this study. The specimens were analyzed and classified on the basis of absorbance analysis, using two simultaneously recorded videocamera images processed via computer using standard software. Immunoreactivity was quantified on the basis of the assumption that the total absorbance was directly proportional to the immunoreactivity. The microscope camera was operated utilizing the Lambert–Beer law, using applicable calibration and controls yielding appropriate linearity between light and dark settings. The measurements were made at wavelengths of 500 and 620 nanometers.

Total collagen deposition was estimated by determining the size of the area with positive staining exceeding a preset threshold level and reporting the ratio of the area relative to the total area analyzed. The procedure was carried out using a modification of the QPI program (Becton-Dickinson, Leiden, The Netherlands) as follows: The appropriate background light intensity and corresponding antibody levels were calibrated. Negative fibers were selected from appropriate areas of the specimen. Measurements were recorded for fibers fulfilling the criteria of morphological alteration, thus excluding contaminating populations. Absolute values of total optical density, indicating antibody-staining intensity, were recorded and reported as such. Staining intensity, shape, size and location of individual fibers were also assessed, using a modification of the CMP program (Becton-Dickinson, Leiden, The Netherlands). The procedure was carried out as follows: Each fiber was measured by using the "classify" function. Background light was calibrated using the automated function. Background thresholds and antibody thresholds were set on the basis of visual inspection. As the background control, the total area was measured and the same procedure was repeated with the antibody-treated area. The total area measured exceeded 65, 536 pixels. Fiber size, the shape factor (the ratio of squared perimeter to cell area), determining fiber irregularity, and the integrated optical density, determining antibody staining intensity, were recorded.

Statistical Methods

Statistical analysis of the significance of alterations of cell properties in different lesions was performed using SPSS for Windows Release 8.0.1 (SPSS Inc, Chicago, Illinois USA). Means, standard deviations and 95% confidence intervals of means were calculated for size, shape, and intensity of individual collagen-staining fibers in different lesions. Tests for normality were carried out using the Kolmogorov–Smirnov test. When normality tests were passed, one-way ANOVA as well as the Kruskall–Wallis H test were used. When Levene's test for homogeneity of variance was significant, Dunnett's T3 test was used for post hoc pair-wise analysis. Statistical comparison of areas of positive staining in different lesions was carried out after the Kolmogorov–Smirnov test showed normality of the data. One-way ANOVA was significant ($p = 0.008$), as was the Kruskall–Wallis H-test ($p = 0.016$), showing differences between groups. With Levene's test for homogeneity of variance significant ($p = 0.024$), Dunnett's T3 test was used for post hoc pair-wise analysis, and no significant differences between pairs were detected. Regression analysis showed the correlation between collagen shape and size to be statistically significant (Pearson's correlation coefficient $= 0.74$; $p < 0.0005$).

RESULTS

Tumor Development

The incidences of the different types of respiratory tract tumor encountered in this study are shown in Figure 1. The respiratory tumor incidence was high in groups 1 and 2. In

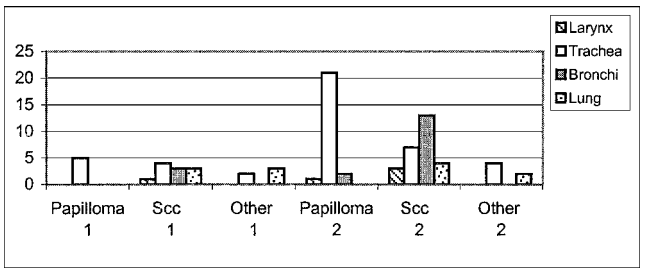

FIGURE 1.—Numbers of different types of tumor in different locations in hamsters, induced by DBC. 1 = group 1 (received 30 mg), 2 = group 2 (received 9 mg). SCC-squamous cell carcinoma.

group 1, a total dose of 30 mg caused 27 tumors in 19 out of 45 animals, the tumors being located mainly in the trachea and bronchi. The mean latency period for tumors in group 1 was 41 weeks. The first tumor, a squamous cell carcinoma of the larynx, was seen in an animal that died at week 31. In group 2 a total dose of 9 mg caused tumors in 33 of 45 animals. Many animals had multiple tumors, yielding a total of 72 tumors in this group. Most of the tumors (55%) were located in the trachea and bronchi. The mean latency period in group 2 was 32 weeks, the first malignant tumor being seen in the trachea at week 26. In both groups, the morphological types were mainly papillomas and squamous cell carcinomas, with a small number of adenocarcinomas and neoplasms of the pulmonary lining.

Tracheobronchial Preneoplastic Lesions

Tracheobronchial epithelium exposed to DBC showed a number of preneoplastic and neoplastic lesions with associated alterations of the ECM. The first changes appearing in DBC-exposed upper respiratory tract (larynx and trachea) were squamous metaplasia, basal cell hyperplasia and dysplasia (Figure 2A). Collagen synthesis was increased in DBC-induced dysplasia, as reflected in an increased number of grains in the subepithelial ECM in in situ hybridization (Figure 2B), indicating accumulation of type I procollagen mRNA.

Basement membrane thickening and disruption (Figure 3A) were associated with an increase in collagens, increasing in extent with severity, from moderate (Figure 3B) to severe. Expression of smooth muscle antigen-positive myofibroblasts also increased in dysplasia (Figure 3C).

Tracheobronchial Benign Tumors

The first tracheobronchial tumors to appear were papillomas (Figure 2C), consisting of proliferating epithelium ultimately invading the stroma. The connective tissue stalk contained PINP-positive type I collagen and PIIINP-positive type III collagen. The total amount of collagen, as indicated by reticulin staining, was increased in the subepithelial area beneath the BM. In papillomas, the mRNA levels for type I (Figure 2D) and type III collagens (Figure 2E) were higher than those observed in simple dysplasia, forming a sheet-like band below the BM. Smooth muscle antigen (SMA) expression was also distinct, indicating the occurrence of myofibroblasts.

Tracheobronchial Squamous Cell Carcinomas

The predominant tumor type induced by DBC in the trachea and bronchi was squamous cell carcinoma (SCC) (Figure 1) of varying degrees of differentiation. Slowly growing, malignant, well-differentiated grade 1 carcinomas consisted of solid sheets of squamous cells with large horn cysts in a collagen-containing ECM. Collagen type I mRNA (Figure 2F) and type III mRNA signals, as measured by in situ hybridization, were distinct in the stroma in the immediate vicinity of the epithelial tumor islets.

Malignant progression was associated with a distinct increase in deposition of ECM fibrillary components. Thick, occasionally hyalinized bundles of filamentous structures positive for type I procollagen were observed in the stroma adjacent to the epithelial structures (Figure 3D), compared with controls (Figure 3E). These neoplasms exhibited an expansive growth pattern, with collagen type I- and collagen type III-containing reticulin in the immediate vicinity of the epithelial tumor cells.

Moderately differentiated, grade 2, squamous cell carcinomas consisted of squamous cells with individual keratinization arranged in islets extending into the surrounding ECM (Figure 2G). Ultrastructural analysis revealed irregular filamentous structures in the tumor stroma (Figure 2H). Collagen type I mRNA and type III mRNA signals were localized to the ECM more distantly than the epithelial islets (Figure 2I).

A decrease in degree of differentiation of squamous cell carcinomas was associated with a decrease in deposition of collagens adjacent to epithelial islets. A decrease of PIIINP-positive type III procollagen fibers and PINP-positive type I procollagen fibers and destruction of ICTP-positive procollagen type I fibers (Figures 3F,G) was observed in the ECM adjacent to epithelial islets.

In less-differentiated (grade 3) neoplasms, ECM development was less distinct. These tumors consisted of irregular hyperchromatic cells devoid of glandular arrangements or keratin expression. The tumor islet cells were surrounded by loose ECM (Figure 2J), containing fairly few fibers. Collagen synthesis, as measured by in situ hybridization for collagen types I and III when compared with controls (Figure 2K), was less distinct (Figure 2L).

Solid tumor islets were associated with aberrant ECM, with thick irregular fibers, significantly larger than those in unaltered matrix (Figures 3H, 3I), consisting of collagen type I- and type III-containing reticulin. Reticulin-positive fibers were more distinct, indicating the occurrence of collagenous filaments other than typical type I and type III collagens. Deposits of myofibroblasts were less distinct, as revealed by scanty staining for SMA (Figure 3J).

Alveolar Neoplasms

Epithelial neoplastic growth along alveolar surfaces was also distinct. The lungs in both groups bore diffuse, or sometimes focal, peripheral proliferative lesions, which developed around the bronchus and followed the alveolar structure an adenomatoid pattern (Figure 4A). Glandular structures exhibited distinct cytological atypia and a scanty ECM (Figure 4B).

These adenocarcinomas showed a prominent but thin ECM containing collagen type I (Figure 5A) and type III. Growth into surrounding stroma produced an increase in collagen deposits (Figure 5B) and smooth muscle antigen-positive

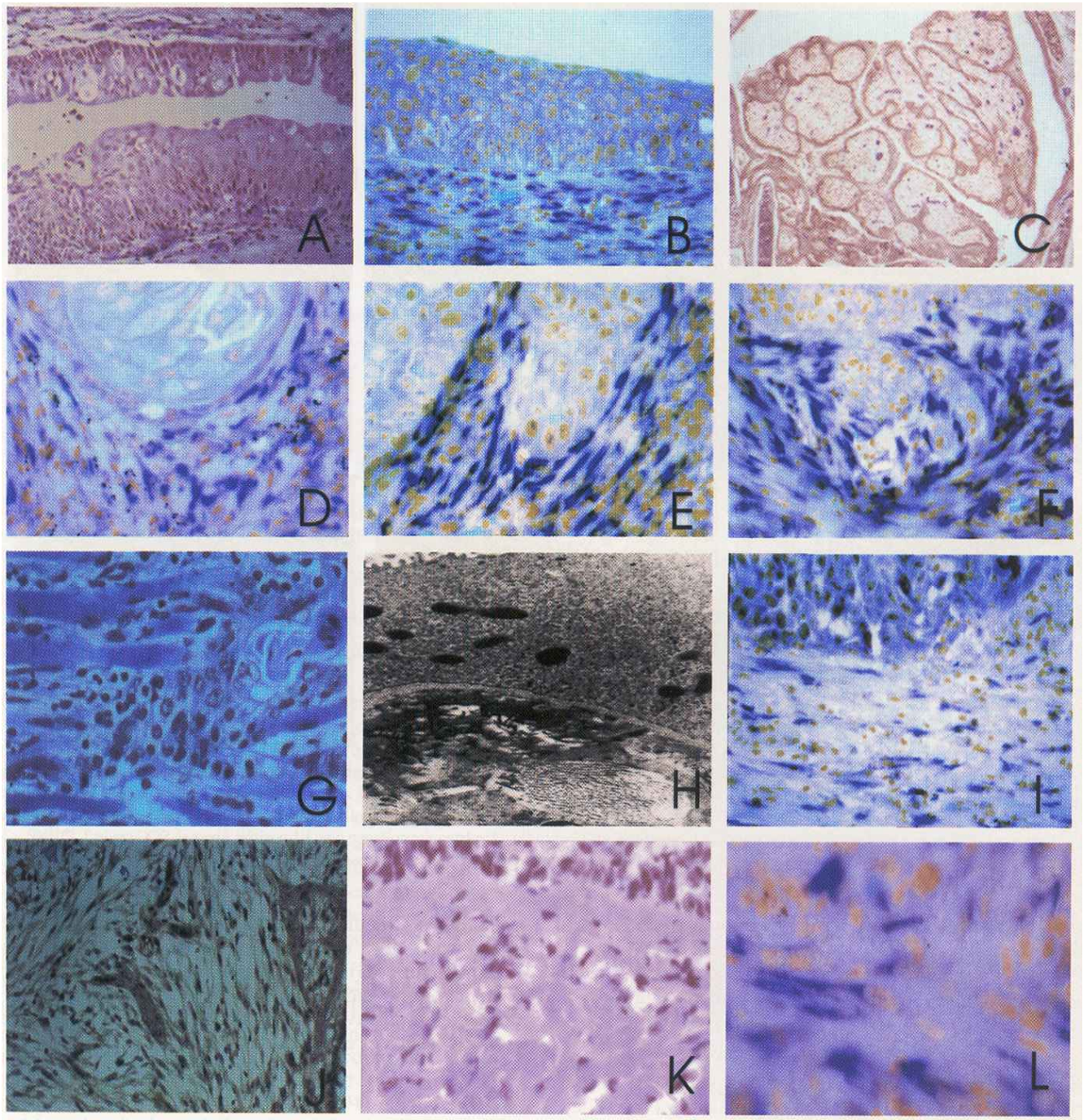

FIGURE 2.—Histopathology of DBC-induced respiratory tumors. A = moderate and severe dysplasia in the tracheobronchial epithelium, H&E. ×500, B = Collagen synthesis in ECM of dysplasia, α1(I) mRNA, digoxigenin in situ hybridization ×500, C = tracheobronchial papilloma, H&E. ×250, D = Collagen synthesis in papilloma, α1(I) mRNA, digoxigenin in situ hybridization, ×500, E = Collagen type III synthesis in stroma around papilloma epithelium, α1(III) mRNA, digoxigenin in situ hybridization ×500, F = Collagen synthesis in stroma around invading epithelial islet of SCC grade 1, α1(I) mRNA, digoxigenin in situ hybridization ×500, G = Epithelial cells of SCC grade 2 invading surrounding ECM, HE ×500, H = High-power view of collagen deposits in SCC grade 2, uranyl acetate-lead citrate ×20,000, I = Collagen synthesis in distant areas of ECM of SCC grade 2, α1(I) mRNA, digoxigenin in situ hybridization ×500, J = Loose stroma in SCC grade 3, alcian blue ×250, K = Control specimen of radioactive in situ hybridization, ×500. L = Irregular collagen synthesis in ECM of SCC grade 3, α1(I) mRNA, digoxigenin in situ hybridization ×500.

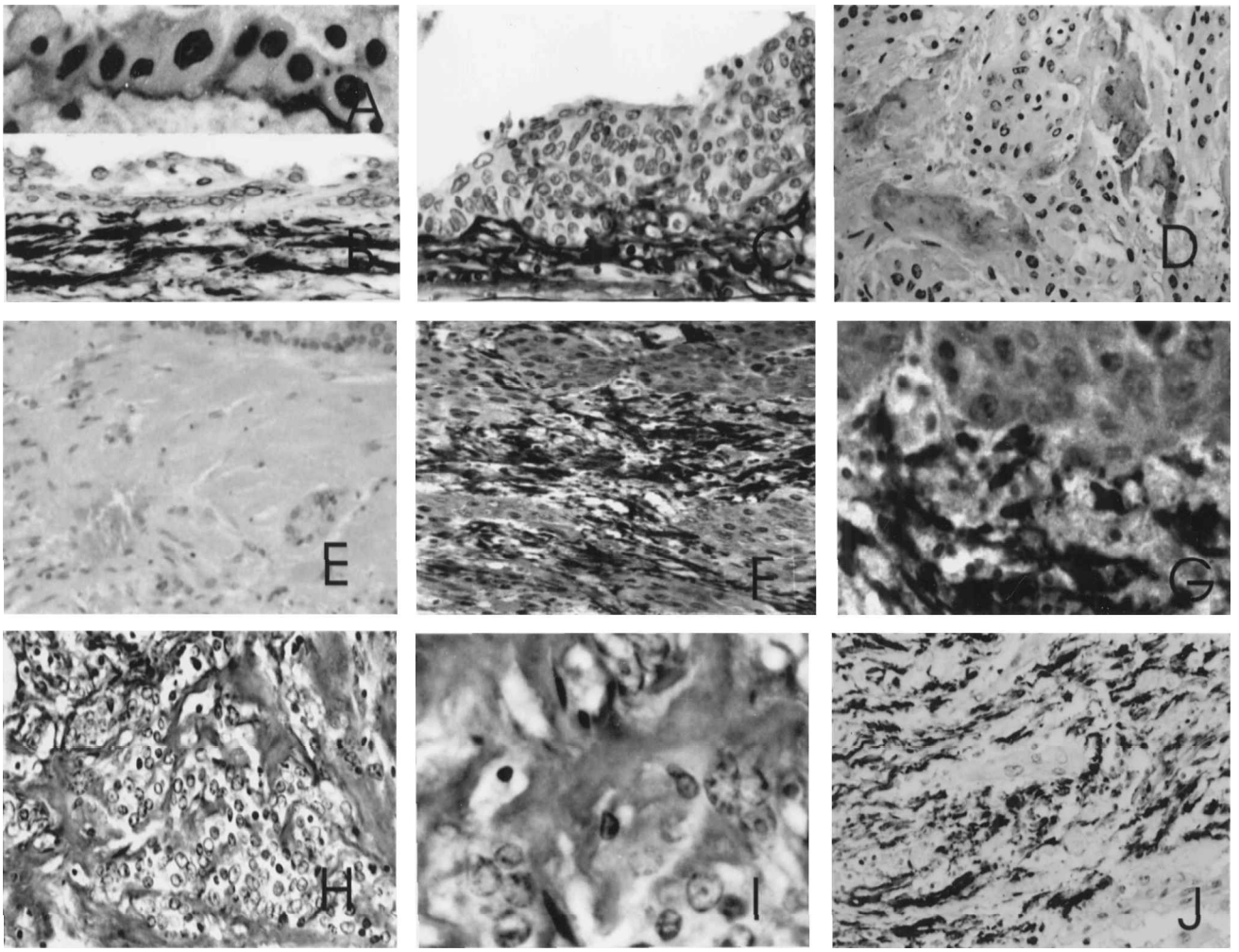

FIGURE 3.—Collagen staining in ECM of tracheobronchial epithelium and neoplasms. A = irregular, discontinuous BM in dysplasia, laminin ×600, B = Collagen type III deposits in moderate dysplasia, PIIINP ×500, C = Smooth muscle antigen-expressing myofibroblasts in severe dysplasia, SMA ×500, D = Collagen type III deposits in stroma of SCC grade 1, PIIINP ×240, E = Control specimen, PIIINP ×250, F = Mature type I collagen fibers surrounding epithelial islets in SCC grade 2, ICTP ×240, G = High-power view of the same tumor as in Figure 3F, ICTP ×1,000, H = Irregular collagen type III-positive fibers in SCC grade 2, PIIINP ×240, I = High power view of the same tumor as in Figure 3H, PIIINP ×1,000, J = smooth muscle antigen expression in SCC grade 3, SMA ×240.

myofibroblasts (Figure 5C). Extended growth and increased cellular atypia was associated with deposits of irregular collagen-containing reticulin-positive structures (Figure 5D) with discontinuous thickened or club-like fibers (Figure 5E).

Neoplasms of the Pulmonary Lining Surface

Epithelial proliferative lesions of the pulmonary lining surface were lesions with a different collagen profile. They exhibited cellular atypia, nuclear irregularities and hyperchromatism. These nodular excrescences of the pulmonary lining contained fibrillary as well as epithelial (Figure 4C) components. These lesions progressed to malignant neoplasms invading the lung. Fully developed neoplasms consisted of pleomorphic cells with sparse keratin formation, arranged in diffuse cords in the stroma (Figure 4D). Collagen type I mRNA (Figure 4E) and type III mRNA (Figure 4F) signals, as measured by in situ hybridization, were distinct in the stroma in the immediate vicinity of the epithelial tumor islets.

Collagen structures formed an intimate part of the neoplasm, and more differentiated neoplasms also contained mucin (Figure 5G). The ECM consisted of irregular, thickened, type I- and type III-positive fibers (Figure 5H). Procollagen-positive structures were arranged in bundles encircling groups of epithelial cells (Figure 5I).

Morphometric Characteristics of Collagenous ECM

The size of the area of collagen exceeding the predetermined threshold in relation to the total area of the lesion was measured by automated image analysis. The total volume of collagen as measured by the CAS200 QPI program was related to the stage of neoplasm development (Figure 6). The data indicated an increase in collagen volume from the nonneoplastic state to dysplasia and further to well differentiated squamous cell carcinoma. Total collagen volume decreased with increasing degree of malignancy from well-to moderately differentiated squamous cell carcinoma, and in less-differentiated neoplasms.

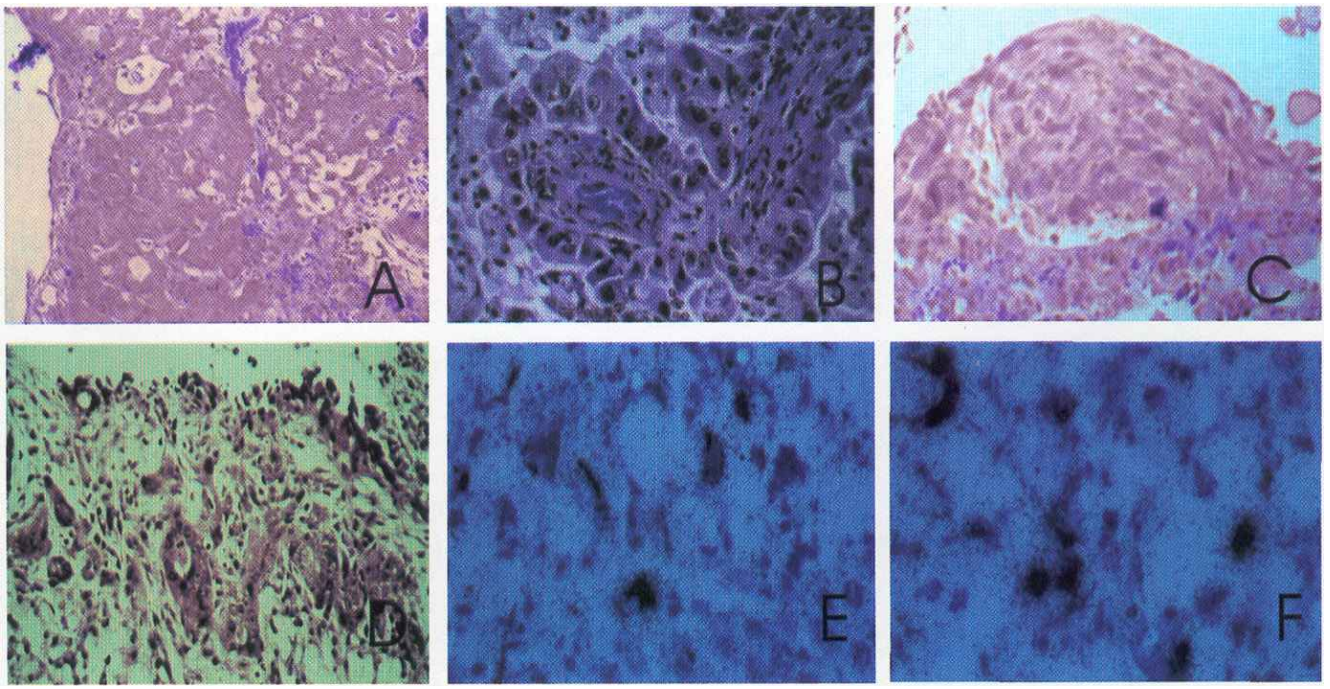

FIGURE 4.—Histopathology of glandular and pleural neoplasms. A = Adenocarcinoma showing epithelial atypia and scanty ECM, HE ×250, B = Papillary arrangements of epithelial cells in adenocarcinoma, HE ×400, C = Epithelial atypia and proliferating stroma in fibroepithelial tumor of the pleural surface, HE ×400, D = epithelial component of fibroepithelial neoplasm of the pulmonary lining, alcian blue ×250, E = Collagen synthesis in fibroepithelial neoplasm of the pulmonary lining, α1(I) mRNA, radioactive in situ hybridization, ×500, F = Collagen synthesis in fibroepithelial neoplasm of the pulmonary lining, α1(III) mRNA, radioactive in situ hybridization, ×500.

Morphometric Characteristics of Individual Collagen Fibers

Collagen structure, size and shape were also measured by computer-assisted image analysis of collagen type III-positive fibers. Morphometric values were distinctly dependent on the morphological type of the lesion (Figure 7).

The average optical density, indicating intensity of staining of type III collagen (Figure 7A), showed increased immunoreactivity in dysplasia and in well-differentiated squamous cell carcinoma, similarly to the increase in total collagen, as previously described. A decrease in staining intensity was observed in relation to the dedifferentiation of squamous cell carcinomas, similarly to the decrease in total collagen volume.

Fiber size, the area of positive PIIINP staining of individual fibers, is reported as the ratio of collagen fiber size in the lesion studied to the mean of collagen fiber size in normal tissue (Figure 7B). Altered size of collagen fibers was most distinct in moderately differentiated carcinomas, indicating proliferation of aberrant collagens. Collagen deposits were also irregular in undifferentiated small cell neoplasms. The ECM in these neoplasms consisted of accumulations of tiny fibers (Figure 7B). Quantitative alterations in collagen shape specific to the different lesions were not identified (Figure 7C), possibly as a result of the occurrence of different types of collagen fiber in any one area.

To determine the characteristics of individual collagen fibers, the mean, standard deviation and 95% confidence intervals of the means were calculated for measurements of size, shape and intensity of collagen staining in image analysis. Fiber shape alterations increased with increased fiber size (Figure 8) Comparison of collagen staining intensity and fiber size showed the staining intensity to be similar regardless of fiber size. Comparison of staining intensity and fiber shape also yielded a similar result, with staining intensity being similar in fibers of different shape.

Expression of TGFβ

To examine the role of collagen synthesis regulation and collagen deposition, the expression of TGFβ immunoreactivity (Figure 9) was examined and compared with morphology, cell proliferation, and *p*53 expression. The tumors were stained through the use of antibodies to isoenzymes of TGFβ (TGFβ1, TGFβ2, and TGFβ3) and the staining pattern was compared with localization of the *p*53 antibody CM5 and the PCNA antibody PC10.

In metaplastic and hyperplastic tracheobronchial epithelia, TGFβ1 immunoreactivity was strong in surface epithelial cells. In dysplasia, TGFβ1 immunostaining was absent in tracheobronchial epithelial cell layers, showing cytological atypia. TGFβ2 stained epithelial cell layers (Figure 10A) that expressed PCNA and *p*53, whereas TGFβ3 was more distinct in the superficial cell layers (Figure 10B). TGFβ3 staining was localized to superficial epithelial structures (Figure 10C); less so in dysplastic cells. TGFβ3 expression was also distinct in the stroma immediately beneath the epithelium in areas of increased collagen deposition and increased numbers of myofibroblasts, as indicated by increased staining for SMA (Figure 3C).

In well-differentiated squamous cell carcinomas, TGFβ1-positive nuclei were most numerous in perimembranous locations in the central cell layers (Figure 10D), which were

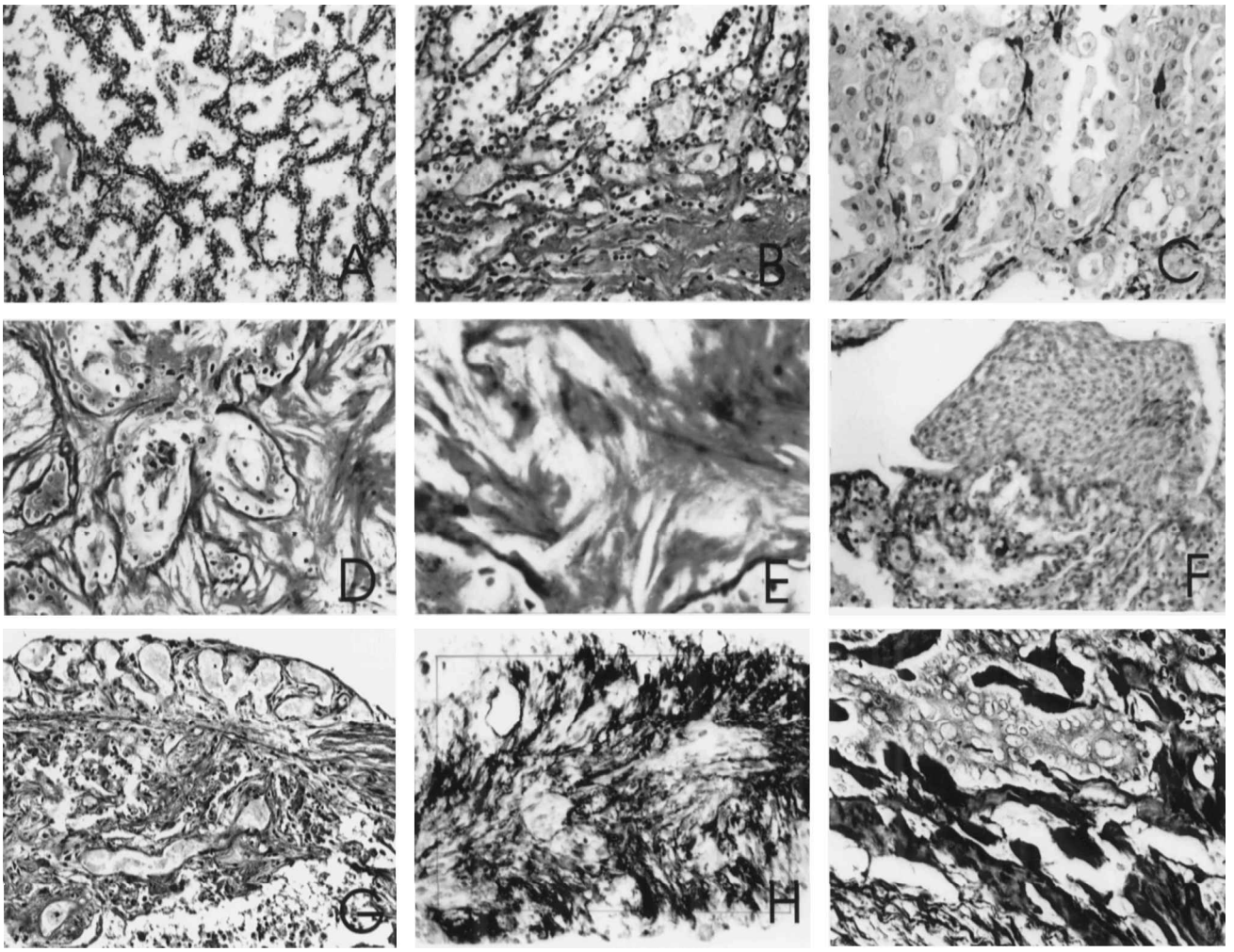

FIGURE 5.—Collagen deposits in glandular and pleural neoplasms. A = Thin, regular collagen type I-positive network in adenocarcinoma, PINP ×240, B = Collagen type III deposits in stroma surrounding adenocarcinoma, PIIINP ×240, C = Smooth muscle antigen-positive myofibroblasts in adenocarcinoma, SMA ×240, D = Reticulin-positive structures in adenocarcinoma, reticulin ×240, E = High power view of irregular collagen deposits in adenocarcinoma, reticulin ×600, F = Fibroepithelial nodule expressing collagen type I, PINP ×240, G = Epithelial structures expressing mucin in collagenous stroma of fibroepithelial tumor, Ab-Pas ×240, H = Collagen type III-staining fibers in fibroepithelial neoplasm of the pulmonary lining, PIIINP ×240, I = Reticulin-positive irregular collagen structures in fibroepithelial tumor, reticulin ×240.

devoid of PCNA immunoreactivity. TGFβ2 stained atypical cells (Figure 10E), which were also positive for PCNA and *p*53. Increased TGFβ3 immunoreactivity occurred in the stroma (Figure 10F) concomitantly with an increase in collagen deposition, being prominent in malignant cells invading the surrounding stroma. In moderately well-differentiated neoplasms (Figure 10G), TGFβ2 expression was observed in neoplastic cells. In less well-differentiated neoplasms, TGFβ2 expression remained in a few malignant cells (Figure 10H), whereas TGFβ3 activity remained in alveolar ECM (Figure 10I). Automated image analysis of TGFβ expression showed increased TGFβ1 expression in epithelium compared with stroma (Figure 9A). No distinct correlation to lesion morphology was observed, however. TGFβ2 expression increased in proliferating epithelial cells during neoplasm progression (Figure 9B), occurring in cells expressing PCNA and *p*53. TGFβ2 immunoreactivity was present in most tumor cells, being lower in the ECM and in differentiated horn pearls in well differentiated squamous cell carcinomas. TGFβ3 expression was distinct in the ECM (Figure 9C) and in tumor cells.

DISCUSSION

A distinct increase in the amount of fibrillary structures in the adjacent stroma was characteristic of preneoplastic tracheobronchial lesions, epithelial hyperplasia and dysplasia, in this study. These early occurring alterations in the ECM have not been previously described in this manner and could partly explain the rapid progression of respiratory tracheobronchial epithelial lesions. In well differentiated squamous cell carcinomas of the lung, an increase in collagen deposition and synthesis was distinct, as in other human neoplasms (26). In this expansive growth pattern, interstitial collagens were distributed as thick bands adjacent to the epithelial border, with distinct staining of PINP and PIIINP. This could also be interpreted as a host defense mechanism inhibiting the spread of the neoplasm (26).

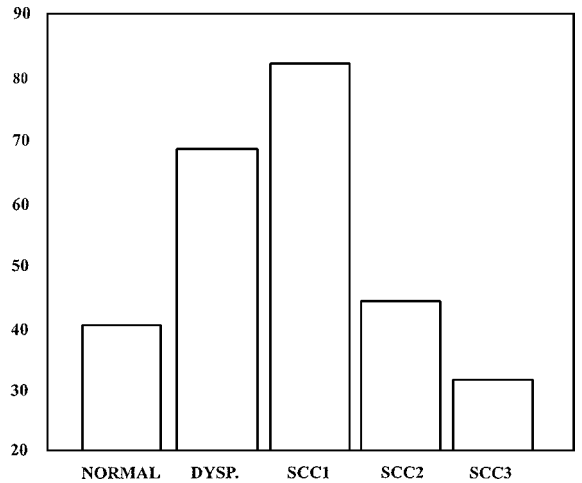

FIGURE 6.—Size of area expressing PIIINP-positive staining in tracheobronchial ECM and in neoplasms as measured by the CAS200 QPI program. Normal = exposed, morphologically unaltered, Dysp = dysplasia, SCC 1 = well-differentiated squamous cell carcinoma, SCC II = moderately differentiated squamous cell carcinoma, SCC III = less-differentiated squamous cell carcinoma.

Distinct irregular collagen deposits were hallmarks of the ECM in moderately differentiated squamous cell carcinomas. Focal collagen fiber destruction and a decrease in the positive staining of fibers were observed in the immediate vicinity of invading tumor islets. Collagen destruction could be due to the action of enzymes, such as metalloproteases (63, 66). The action of these enzymes has been considered a prerequisite for tumor growth and progression, as seen in other types of tumor in man (26) and experimental animals (62). In less-differentiated squamous cell carcinomas, the matrix components and isolated squamous cells were occasionally mixed. Areas of matrix disintegration, cellular proliferation, and the formation of abortive structures occurred in the same neoplasm (27). This finding is consistent with the concept that tumor stroma actively participates in malignant progression (3, 30, 73). The stage-dependent alterations in volume and structure of specific ECM components have not been previously described.

Characteristics of individual fibers were also assessed in this study, revealing alterations related to neoplastic growth pattern and degree of tumor differentiation. Collagen staining intensity was increased in moderately differentiated squamous cell carcinomas and decreased with decreasing degree of differentiation. Collagen fiber size was also increased, decreasing in less differentiated squamous cell carcinomas. These findings are consistent with previously presented findings on matrix participation in tumor growth (26, 27). Collagen shape alterations failed to show correlation to tumorigenesis, possible because of the large variations in cell structure in the different lesions.

Image analysis of characteristics of collagen fibers showed staining intensity to be similar in fibers of different sizes and shape; thus, specific quantitative staining characteristics of fibers were not observed. Shape alterations increased with increasing fiber size, indicating concomitant development of aberrations in neoplastic progression. The morphometric characteristics of collagen fibres are mostly unknown, and

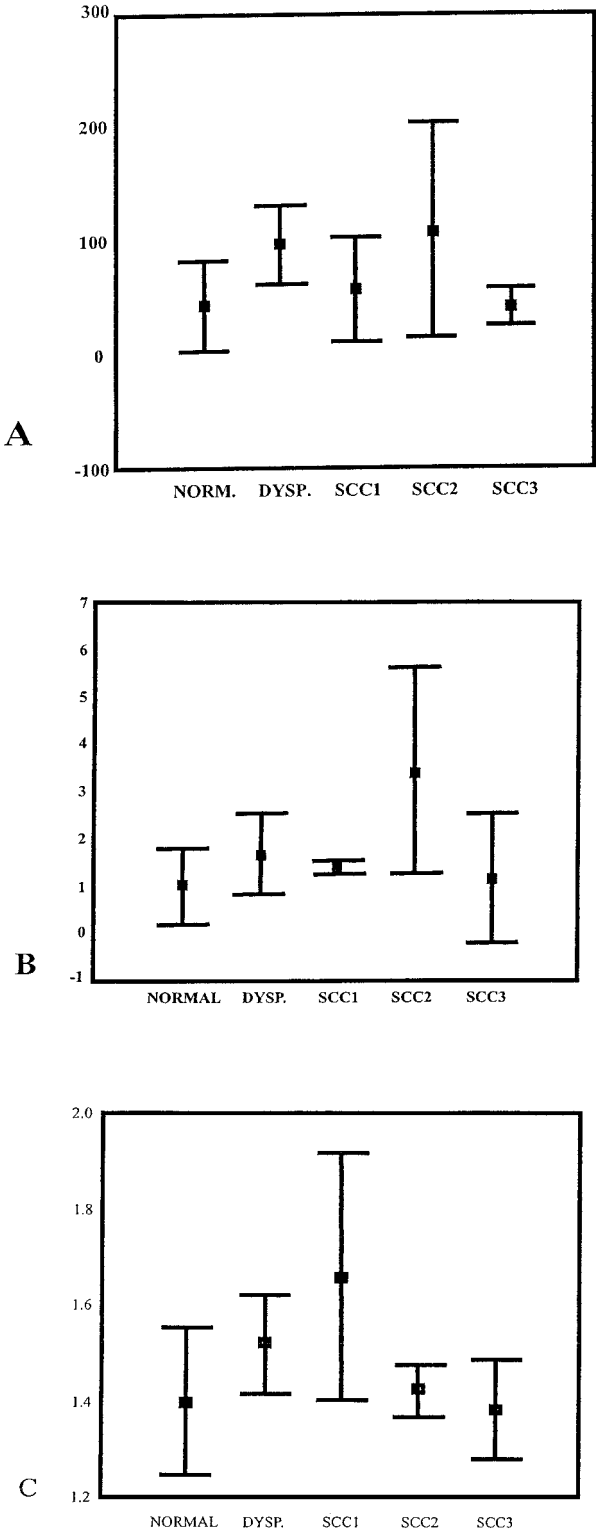

FIGURE 7.—Morphometric analysis of PIIINP-positive collagen fibers in different types of tracheobronchial lesion. Norm = exposed, morphologically unaltered, Dysp = dysplasia, SCC 1 = well-differentiated squamous cell carcinoma, SCC II = moderately differentiated squamous cell carcinoma, SCC III = less differentiated squamous cell carcinoma, A = Staining intensity measured as optical density of PIIINP-positive staining fibers, B = Area indicating size of PIIINP-positive staining fibers, C = Ratio of perimeter to fiber size, indicating shape of PIIINP-positive staining fibers.

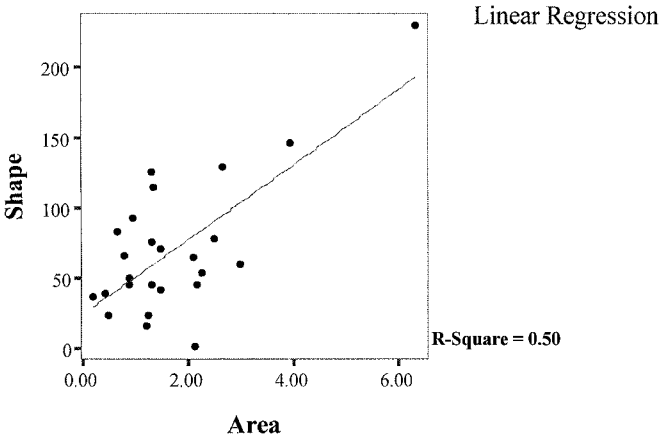

FIGURE 8.—Morphometric analysis of PIIINP-positive collagen fibers. Ratio of fiber shape in relation to fiber size.

further studies are needed to determine the clinical significance of these findings.

Altered TGFβ expression was associated with malignancy in lung tumor development, as in human neoplasia (6, 32, 41, 65, 67). Five distinct TGFβ genes, designated TGFβ1–5, have been identified (31). Each gene encodes a distinct peptide, which dimerizes to form an inactive TFGβ precursor protein. Each TGFβ is secreted as a latent complex, in association with its latency-associated peptide. TGFβ immunoreactivity was associated with neoplastic progression depending upon isoform, in this study. TGFβ1 was present in differentiated cells, as in skin carcinogenesis (9, 11, 15, 18, 71), whereas little or no reactivity was found in undifferentiated small cell tumors, as reported earlier (32). TGFβ2 expression, observed in malignant lung tumor cells in this study, is frequently associated with an unfavorable prognosis in man (6, 32, 41, 65, 67). TGFβ3 expression was also observed in the matrix in this study, and this isoform has also been implicated in collagen formation (19).

The automated image analysis system used in this study made possible accurate, reproducible measurements in a large amount of material. Quantitative morphometric techniques have proved to be useful for immunohistochemical characterization of neoplasms, eg, breast (1, 10) and renal cancers (28). Studies using automated image analysis in classification of neoplasms (70) have shown a sensitivity of 85% to 99%, a specificity of 86% to 98% and a positive predictive value of 87% to 97%. Variability in automated image analysis (42) has been due to specimen variability in systematic sampling in 92% of the cases and specimen variability in selective sampling in 67%. Technical variability has been responsible for 10% of the differences. The importance of sampling schemes and selection criteria has been shown (58). Compared with visual scoring methods, automated image analysis is an improvement (5, 54), provided that adequate precautions are taken. Immunohistochemical analysis is also associated with other problems, eg, relating to specificity and sensitivity of antibodies, effect of fixation on preservation of epitopes, duration of antibody exposure, effect of pretreatments and role of antibody enhancement procedures (62).

The results of the present experiments show the highly carcinogenic effects of DBC, making it useful for the

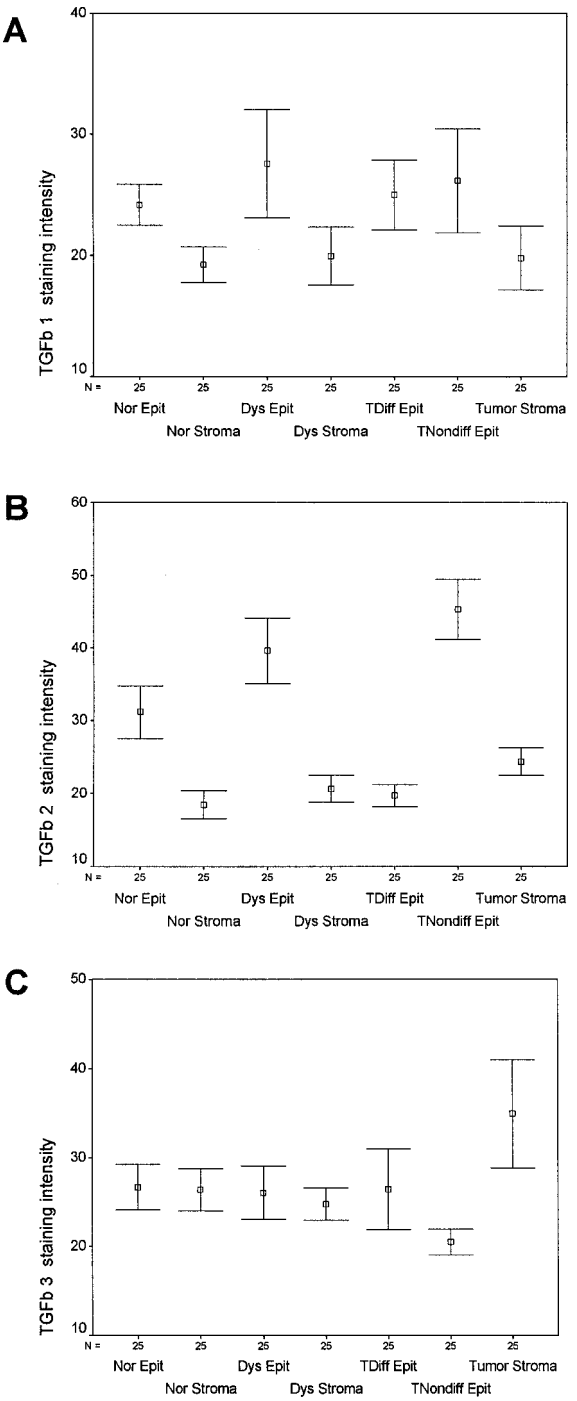

FIGURE 9.—Total areas of TGFβ1 (A), TGFβ2 (B) and TGFβ3 (C) -positive staining in tracheobronchial ECM and in neoplasms. Nor Epit = normal, morphologically unaltered epithelium, Nor Stroma = normal, morphologically unaltered stroma, Dys Epit = dysplasia, epithelium, Dys Stroma = dysplasia, stroma, Tdiff Epit = squamous cell carcinoma moderately and well-differentiated, T Nondiff Epit = undifferentiated squamous cell carcinoma, epithelium, Tumor stroma = squamous cell carcinoma stroma.

experimental induction of respiratory tract tumors (55–57). A total dose of only 9 mg caused more malignant respiratory tract tumors in hamsters, 72%, than have been found in the classical model using B(a)P and Fe_2O_3, where only 30% of the animals had tumors (36). Tumor formation was not

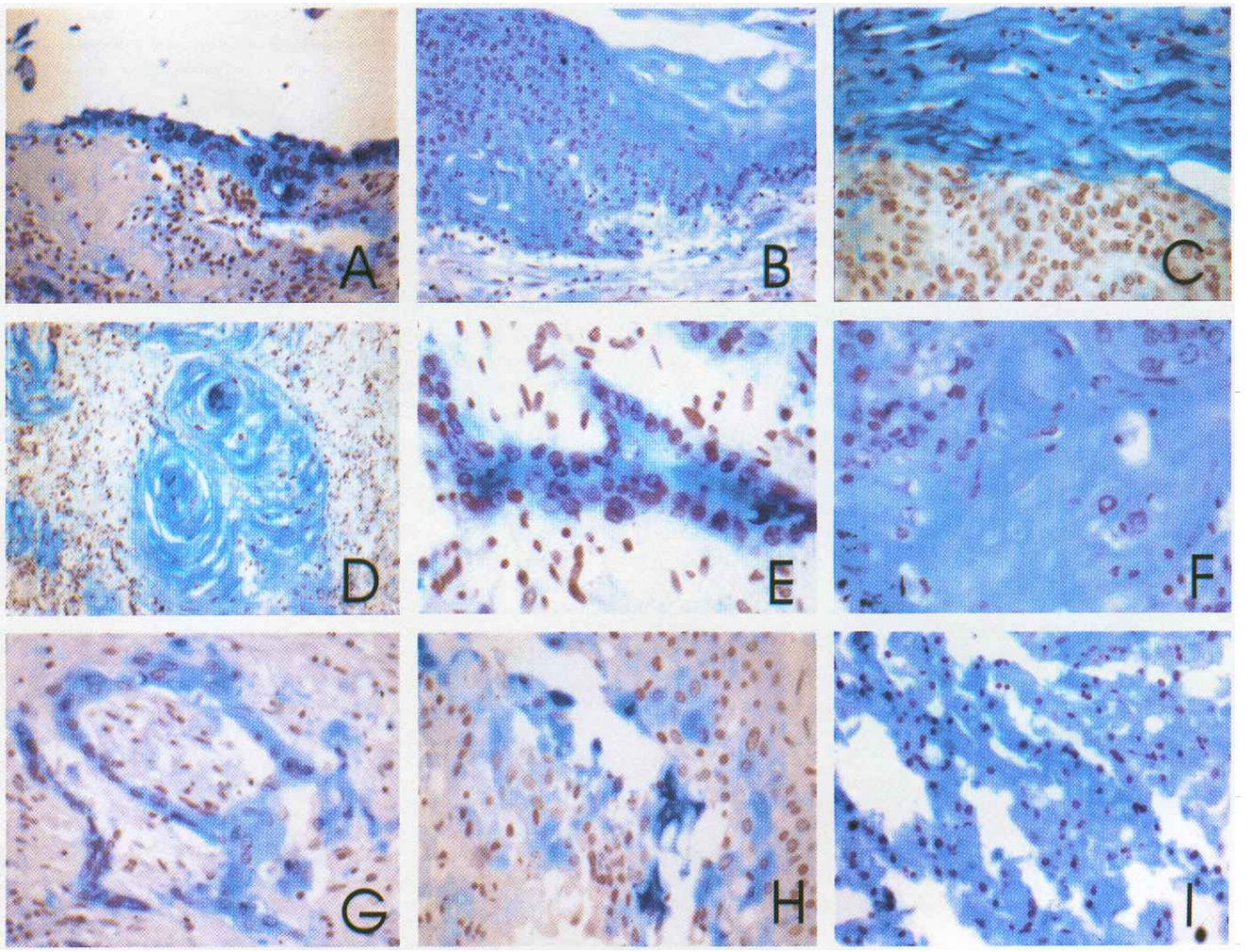

FIGURE 10.—TGFβ immunoreactivity in tracheobronchial epithelium and squamous cell carcinoma. A = TGFβ2 immunoreactivity in dysplastic tracheobronchial epithelium, TGFβ2 ×500, B = TGFβ3 immunoreactivity in dysplastic tracheobronchial epithelium, TGFβ3 ×600, C = TGFβ2 immunoreactivity in dysplastic tracheobronchial epithelium, TGFβ2 ×600, D = TGFβ1 immunoreactivity in tumor cells in well differentiated squamous cell carcinoma, TGFβ1 ×240, E = TGFβ2 immunoreactivity in tumor cells in moderately well differentiated squamous cell carcinoma, TGFβ2 ×600, F = TGFβ3 immunoreactivity in stroma of moderately differentiated squamous cell carcinoma, TGFβ3 ×400, G = TGFβ2 immunoreactivity in tumor cell in moderately well-differentiated squamous cell carcinoma, TGFβ2 ×400, H = TGFβ2 immunoreactivity in tumor cells in less well differentiated squamous cell carcinoma, TGFβ2 ×500, I = TGFβ3 immunoreactivity in alveolar ECM of moderately differentiated squamous cell carcinoma, TGFβ3 ×240.

dose-dependent (group 1 vs group 2) in this study. The lower dose was more carcinogenic, possibly due to the toxic effects of DBC on the tracheobronchial surface epithelium. Morphologically, the tumors in this study were similar to those seen in man. Most neoplasms were squamous cell carcinomas, and the stem bronchi and trachea seemed to be the preferential sites for the tumors. Adenocarcinomas, less common in this study, showed less distinct ECM changes. Mesotheliomas associated with asbestos exposure in man (69), show similarities to the neoplasms induced by the tobacco component DBC in this study.

In conclusion, the model of respiratory tumor development with known endpoints used in this study showed similarities to human tumor formation, making it a good model for lung cancer research. Stromal changes occurring during tumor development were directly associated with the neoplastic response, increasing with increasing degree of malignancy. This may be interpreted as host defense. The minimal collagen deposition seen in small cell tumors could explain the rapid growth of these tumors.

ACKNOWLEDGMENTS

The authors gratefully acknowledge the expert technical assistance in immunohistochemistry of Mrs Riitta Vuento, Mrs Tuula Lujala, Mrs Erja Tomperi, and Mrs Mirja Vahera, the photography and computer analysis carried out by Mr Hannu Väänänen and Mr Tapio Leinonen, the autoradiography carried out by Ms Veera Näyhä, BM, Mrs Annikki Huhtala, and Ms Heli Auno, the statistical analysis carried out by David Harrison and Drs. J. and L. Risteli, Department of Clinical Chemistry, University of Oulu, for Collagen antibodies. The financial support of Oulu University Hospital, the Finnish Cancer Society and Finska Läkarsällskapet, Finland, is gratefully acknowledged.

REFERENCES

1. Albonico G, Querzoli P, Ferretti S, Rinaldi R, Nenci I (1998). Biological profile of *in situ* breast cancer investigated by immunohistochemical technique. *Cancer Detect Prevent* 22: 313–318.
2. An CS, Petrovic LM, Reyter I, Tolmachoff T, Ferrell LD, Thung SN, Geller SA, Marchevsky AM (1997). The application of image analysis and neural network technology to the study of large-cell liver-cell dysplasia and hepatocellular carcinoma. *Hepatology* 26: 1224–1231.
3. Barsky SH, Siegal GP, Jannotta F, Liotta LA (1983). Loss of basement membrane components by invasive tumors but not by their benign counterparts. *Lab Invest* 49: 140–147.
4. Bascom CC, Wolfshohl JR, Coffey RJJ, Madisen L, Webb NR, Purchio AR, Derynck R, Moses HL (1989). Complex regulation of transforming growth factor beta 1, beta 2, and beta 3 mRNA expression in mouse fibroblasts and keratinocytes by transforming growth factors beta 1 and beta 2. *Molecul Cell Biol* 9: 5508–5515.
5. Bejar J, Sabo E, Misselevich I, Eldar S, Boss JH (1998). Comparative study of computer-assisted image analysis and light-microscopically determined estrogen receptor status of breast carcinomas. *Arch Pathol Laborat Med* 122: 346–352.
6. Chaudhry A, Oberg K, Gobl A, Heldin CH, Funa K (1994). Expression of transforming growth factors beta 1, beta 2, beta 3 in neuroendocrine tumors of the digestive system. *Anticanc Res* 14: 2085–2091.
7. Choi Y, Fuchs E (1990). TGF-beta and retinoic acid: regulators of growth and modifiers of differentiation in human epidermal cells. *Cell Regul* 1: 791–809.
8. Coffey RJJ, Derynck R, Wilcox JN, Bringman TS, Goustin AS, Moses HL, Pittelkow MR (1987). Production and auto-induction of transforming growth factor-alpha in human keratinocytes. *Nature* 328: 817–820.
9. Cui W, Kemp CJ, Duffie E, Balmain A, Akhurst RJ (1994). Lack of transforming growth factor-beta 1 expression in benign skin tumors of p53null mice is prognostic for a high risk of malignant conversion. *Cancer Res* 54: 5831–5836.
10. el-Badawy N, Cohen C, Derose PB, Check IJ, Sgoutas D (1991). Immunohistochemical progresterone receptor assay. Measurement by image analysis. *Am J Clin Pathol* 96: 704–710.
11. Escherick JS, DiCunto F, Flanders KC, Missero C, Dotto GP (1993). Transforming growth factor beta 1 induction is associated with transforming growth factors beta 2 and beta 3 down-modulation in 12-O-tetradecanoylphorbol-13-acetate-induce d skin hyperplasia. *Cancer Res* 53: 5517–5522.
12. Flanders KC, Thompson NL, Cissel DS, Van Obberghen-Schilling E, Baker CC, Kass ME, Ellingsworth LR, Roberts AB, Sporn MB (1989). Transforming growth factor-beta 1: Histochemical localization with antibodies to different epitopes. *J Cell Biol* 108: 653–660.
13. Fleischmajer R, Perlish JS, Timpl R (1985). Collagen fibrillogenesis in human skin. *Ann NY Acad Sci* 460: 246–257.
14. Fleischmajer R, Schechter A, Bruns M, Perlish JS, MacDonald ED, Pan TC, Timpl R, Chu ML (1995). Skin fibroblasts are the only source of nidogen during early basal lamina formation *in vitro*. *J Invest Dermatol* 105: 597–601.
15. Fowlis DJ, Flanders KC, Duffie E, Balmain A, Akhurst RJ (1992). Discordant transforming growth factor beta 1 RNA and protein localization during chemical carcinogenesis of the skin. *Cell Growth Different* 3: 81–91.
16. Frank R, Adelmann-Grill BC, Herrmann K, Haustein UF, Petri JB, Heckmann M (1996). Transforming growth factor-beta controls cell-matrix interaction of microvascular dermal endothelial cells by downregulation of integrin expression. *J Invest Dermatol* 106: 36–41.
17. Furness PN (1997). The use of digital images in pathology. *J Pathol* 183: 253–263.
18. Glick AB, Kulkarni AB, Tennenbaum T, Hennings H, Flanders KC, O'Reilly M, Sporn MB, Karlsson S, Yuspa SH (1993). Loss of expression of transforming growth factor beta in skin and skin tumors is associated with hyperproliferation and a high risk for malignant conversion. *Proc Natl Acad Sci USA* 90: 6076–6080.
19. Gold LI, Jussila T, Fusenig NE, Stenback F (2000). TGF-beta isoforms are differentially expressed in increasing malignant grades of HaCaT keratinocytes, suggesting separate roles in skin carcinogenesis. *J Pathol* 190: 579–588.
20. Gold LI, Saxena B, Mittal KR, Marmor M, Goswami S, Nactigal L, Korc, Demopoulos RI (1994). Increased expression of transforming growth factor beta isoforms and basic fibroblast growth factor in complex hyperplasia and adenocarcinoma of the endometrium: Evidence for paracrine and autocrine action. *Cancer Res* 54: 2347–2358.
21. Gorsch SM, Memoli VA, Stukel TA, Gold LI, Arrick BA (1992). Immunohistochemical staining for transforming growth factor beta 1 associates with disease progression in human breast cancer. *Cancer Res* 52: 6949–6952.
22. Heine U, Munoz EF, Flanders KC, Ellingsworth LR, Lam HY, Thompson NL, Roberts AB, Sporn MB (1987). Role of transforming growth factor-beta in the development of the mouse embryo. *J Cell Biol* 105: 2861–2876.
23. Henry MC, Port CD, Bates RR, Kaufman DG (1973). Respiratory tract tumors in hamsters induced by benzo(a)pyrene. *Cancer Res* 33: 1585–1592.
24. Hoffmann D, Wynder EL (1967). The reduction of the tumorigenicity of cigarette smoke condensate by addition of sodium nitrate to tobacco. *Cancer Res* 27: 172–174.
25. Johnson MD, Federspiel CF, Gold LI, Moses HL (1992). Transforming growth factor-beta and transforming growth factor beta-receptor expression in human meningioma cells. *Am J Pathol* 141: 633–642.
26. Kauppila S, Saarela J, Stenback F, Risteli J, Kauppila A, Risteli L (1996). Expression of mRNAs for type I and type III procollagens in serous ovarian cystadenomas and cystadenocarcinomas . *Am J Pathol* 148: 539–548.
27. Kauppila S, Stenback F, Risteli J, Jukkola A, Risteli L (1998). Aberrant type I and type II collagen gene expression in human breast cancer *in vivo*. *J Pathol* 186: 262–268.
28. Khurana KK, Truong LD, Verani RR (1998). Image analysis of proliferating cell nuclear antigen expression and immunohistochemical profiles in renal cell carcinoma associated with acquired cystic kidney disease: Comparison with classic renal cell carcinoma. *Mod Pathol* 11: 339–346.
29. Levine JH, Moses HL, Gold LI, Nanney LB (1993). Spatial and temporal patterns of immunoreactive transforming growth factor beta 1, beta 2, and beta 3 during excisional wound repair. *Am J Pathol* 143: 368–380.
30. Liotta LA, Kohn E (1990). Cancer invasion and metastases *JAMA* 263: 1123–1126.
31. Massague J (1990). The transforming growth factor-beta family. *Ann Rev Cell Biol* 6: 597–641.
32. McCune BK, Patterson K, Chandra RS, Kapur S, Sporn MB, Tsokos M (1993). Expression of transforming growth factor-beta isoforms in small round cell tumors of childhood. An immunohistochemical study. *Am J Pathol* 142: 49–58.
33. Melkko J, Kauppila S, Niemi S, Risteli L, Haukipuro K, Jukkola A, Risteli J (1996). Immunoassay for intact amino-terminal propeptide of human type I procollagen. *Clin Chem* 42: 947–954.
34. Melkko J, Niemi S, Risteli L, Risteli J (1990). Radioimmunoassay of the carboxyterminal propeptide of human type I procollagen. *Clin Chem* 36: 1328–1332.
35. Mize RR, Holdefer RN, Nabors LB (1988). Quantitative immunocytochemistry using an image analyzer. I. Hardware evaluation, image processing, and data analysis. *J Neurosci Met* 26: 1–23.
36. Montesano R (1970). Systemic carcinogens (*N*-nitroso compounds) and synergistic or additive effects in respiratory carcinogenesis . *Tumori* 56: 335–344.
37. Parekh T, Saxena B, Reibman J, Cronstein BN, Gold LI (1994). Neutrophil chemotaxis in response to TGF-beta isoforms (TGF-beta 1, TGF-beta 2, TGF-beta 3) is mediated by fibronectin. *J Immunol* 152: 2456–2466.
38. Pelton RW, Johnson MD, Perkett EA, Gold LI, Moses HL (1991). Expression of transforming growth factor-beta 1, -beta 2, and -beta 3 mRNA and protein in the murine lung. *Am J Resp Cell Mol Biol* 5: 522–530.
39. Perkett EA, Lyons RM, Moses HL, Brigham KL, Meyrick B (1990). Transforming growth factor-beta activity in sheep lung lymph during the development of pulmonary hypertension. *J Clin Invest* 86: 1459–1464.

40. Querzoli P, Albonico G, Ferretti S, Rinaldi R, Magri E, Indelli M, Nenci I (1996). MIB-1 proliferative activity in invasive breast cancer measured by image analysis. *J Clin Pathol* 49: 926–930.
41. Reed JA, McNutt NS, Prieto VG, Albino AP (1994). Expression of transforming growth factor-beta 2 in malignant melanoma correlates with the depth of tumor invasion. Implications for tumor progression. *Am J Pathol* 145: 97–104.
42. Reeder JE, Cox C, Wheeless LL, Flint A, Liebert M, Grossman HB (1997). Variability of DNA analysis by image cytometry. Bladder Tumor Marker Network. *Cytometry* 28: 176–180.
43. Remmele W, Schicketanz KH (1993). Immunohistochemical determination of estrogen and progesterone receptor content in human breast cancer. Computer-assisted image analysis (QIC score) vs. subjective grading (IRS). *Pathol Res Pract* 189: 862–866.
44. Risteli J, Elomaa I, Niemi S, Novamo A, Risteli L (1993). Radioimmunoassay for the pyridinoline cross-linked carboxy-terminal telopeptide of type I collagen: A new serum marker of bone collagen degradation. *Clin Chem* 39: 635–640.
45. Risteli J, Niemi S, Trivedi P, Maentausta O, Mowat AP, Risteli L (1988). Rapid equilibrium radioimmunoassay for the amino-terminal propeptide of human type III procollagen. *Clin Chem* 34: 715–718.
46. Risteli J, Risteli L (1997). Assays of type I procollagen domains and collagen fragments: Problems to be solved and future trends. *Scand J Clin Lab Invest—Suppl* 227: 105–113.
47. Risteli L, Kauppila A, Makila UM, Risteli J (1988). Aminoterminal propeptide of type-III procollagen in serum—An indicator of clinical behavior of advanced ovarian carcinoma? *Int J Cancer* 41: 409–414.
48. Risteli L, Risteli J (1993). Biochemical markers of bone metabolism. *Ann Med* 25: 385–393.
49. Roberts AB, Sporn MB (1989). Regulation of endothelial cell growth, architecture, and matrix synthesis by TGF-beta. *Am Rev Resp Dis* 140: 1126–1128.
50. Roberts DK, Walker NJ, Parmley TH, Horbelt DV (1988). Interaction of epithelial and stromal cells in vaginal adenosis. *Hum Pathol* 19: 855–861.
51. Saffiotti U, Cefis F, Kolb LH (1968). A method for the experimental induction of bronchogenic carcinoma. *Cancer Res* 28: 104–124.
52. Saffiotti U, Montesano R, Sellakumar AR, Kaufman DG (1972). Respiratory tract carcinogenesis induced in hamsters by different dose levels of benzo-(a)pyrene and ferric oxide. *J Natl Canc Inst* 49: 1199–1204.
53. Schultz CP, Mantsch HH (1998). Biochemical imaging and 2D classification of keratin pearl structures in oral squamous cell carcinoma. *Cell Mol Biol* 44: 203–210.
54. Schultz DS, Katz RL, Patel S, Johnston D, Ordonez NG (1992). Comparison of visual and CAS-200 quantitation of immunocytochemical staining in breast carcinoma samples. *Analyt Quant Cytol Histol* 14: 35–40.
55. Sellakumar A, Shubik P (1972). Carcinogenicity of 7H-dibenzo[c,g]carbazole in the respiratory tract of hamsters. *J Natl Cancer Inst* 48: 1641–1646.
56. Sellakumar A, Shubik P (1974). Carcinogenicity of different polycyclic hydrocarbons in the respiratory tract of hamsters. *J Natl Cancer Inst* 53: 1713–1719.
57. Sellakumar A, Stenback F, Rowland J, Shubik P (1977). Tumor induction by 7H-dibenzo[c,g]carbazole in the respiratory tract of Syrian hamsters. *J Toxicol Environ Health* 3: 935–939.
58. Shiina H, Igawa M, Yagi H, Urakami S, Yoneda T, Shirakawa H, Ishibe (1996). Immunohistochemistry of *p*53 protein in transitional-cell carcinoma of the bladder using an image analyzer. *Oncology* 53: 233–240.
59. Sporn MB, Roberts AB (1988). Peptide growth factors are multifunctional. *Nature* 332: 217–219.
60. Stenback F (1977). Morphology of experimentally induced respiratory tumors in syrian golden hamster. A histological, histochemical and ultrastructural study. *Acta Oto-Laryngol—Suppl* 347: 1–59.
61. Stenback F, Makinen M, Jussila T (1998). *p*53 expression in skin carcinogenesis and its relationship to cell proliferation and tumour growth. *Eur J Cancer* 34: 1415–1424.
62. Stenback F, Makinen M, Jussila T, Kauppila S, Risteli J, Talve L, Risteli L (1999). The extracellular matrix in skin tumor development—A morphological study. *J Cut Patol* 26: 327–338.
63. Stetler-Stevenson WG, Liotta LA, Kleiner DE, Jr. (1993). Extracellular matrix 6: Role of matrix metalloproteinases in tumor invasion and metastasis. *FASEB J* 7: 1434–1441.
64. Tähtelä R, Thölix E. (1996). Serum concentrations of type I carboxyterminaltelopeptide (ICTP) and type I procollagen carboxy- and aminoterminal propetides (PICP, PINP) as markers of metastatic bone disease in breast cancer. *Anticanc Res* 16: 2289–2293.
65. Truong LD, Kadmon D, McCune BK, Flanders KC, Scardino PT, Thompson, TC (1993). Association of transforming growth factor-beta 1 with prostate cancer: An immunohistochemical study. *Hum Pathol* 24: 4–9.
66. van der Stappen JW, Hendriks T, Wobbes T (1990). Correlation between collagenolytic activity and grade of histological differentiation in colorectal tumors. *Int J Cancer* 45: 1071–1078.
67. Walker RA, Dearing SJ (1992). Transforming growth factor beta 1 in ductal carcinoma in situ and invasive carcinomas of the breast. *Eur J Cancer* 28: 641–644.
68. Warshawsky D, Talaska G, Xue W, Schneider J (1996). Comparative carcinogenicity, metabolism, mutagenicity, and DNA binding of 7H-dibenzo [c,g]carbazole and dibenz[a,j]acridine. *Crit Rev Toxicol* 26: 213–249.
69. World Health Organisation, International Agency for Research on Cancer. (1986). Monographs on the evaluation of carcinogenic risks to humans. Tobacco smoking. World Health Organisation, Geneva, Switzerland. Vol 38, pp 1–421.
70. Wojcik EM, Miller MC, O'Dowd GJ, Veltri RW (1998). Value of computer-assisted quantitative nuclear grading in differentiation of normal urothelial cells from low and high grade transitional cell carcinoma. *Analyt Quant Cytol Histol* 20: 69–76.
71. Zenklusen JC, Stockman SL, Fischer SM, Conti CJ, Gimenez-Conti IB (1994). Transforming growth factor-beta 1 expression in Syrian hamster cheek pouch carcinogenesis. *Mol Carcinog* 9: 10–16.
72. Zhu GG, Risteli L, Makinen M, Risteli J, Kauppila A, Stenback F (1995). Immunohistochemical study of type I collagen and type I pN-collagen in benign and malignant ovarian neoplasms. *Cancer* 75: 1010–1017.
73. Zhu GG, Stenback F, Risteli L, Risteli J, Kauppila A (1993). Organization of type III collagen in benign and malignant ovarian tumors. An immunohistochemical study. *Cancer* 72: 1679–1684.